Measurement of the equation of state of solid-density copper heated with laser-accelerated protons

S. Feldman, G. Dyer, D. Kuk, and T. Ditmire

Phys. Rev. E **95**, 031201 — Published 13 March 2017

DOI: 10.1103/PhysRevE.95.031201

Measurement of the equation of state of solid density copper heated with laser accelerated protons

S. Feldman, G. Dyer, D. Kuk, and T. Ditmire

Center for High Energy Density Science, C1510, Department of Physics, University of Texas at Austin, Austin, TX, 78712, USA

We present equation of state (EOS) measurements of solid density copper heated to 5 – 10 eV. A copper sample was heated isochorically by hydrogen ions accelerated from an adjacent foil by a high intensity pulsed laser, and probed optically. The measured temperature and expansion are compared against simulations using the most up-to-date wide range EOS tables available.

PACS numbers: 52.25.Kn, 52.27.Gr, 52.38.Ph, 52.50.Gj

Warm dense matter (WDM) research has seen increasing activity in recent years as new experimental and computational tools allow unprecedented ability to study this difficult regime. Roughly associated with temperatures between 1-100 eV and densities between .1-10 times solid density, WDM presents great challenges both theoretically [1] and experimentally [2]. The relatively high temperature represents particle energy on the order of the Fermi energy, invalidating the classical condensed matter approach of perturbing around a zero temperature, while relatively high density and moderate temperature implies strong coupling between particles so that perturbations from an ideal plasma are likewise inadequate to describe the state. Experimentally, this state of matter is difficult to reach since heating must occur on a timescale faster than the rapid expansion of the plasma. High temperatures and pressures preclude confinement for any appreciable time, so any measurement of this highly transient state must be able to register data from an extremely brief moment in time.

To date, the majority of experimental data relevant to the WDM equation of state (EOS) have come from strong shock experiments, [2-5]. While this class of EOS measurements has played a crucial role in guiding the development of EOS models, it accesses only a narrow range within temperature-density phase space. Recent advances have enabled access to WDM states far from the principal shock Hugoniot through the rapid, isochoric heating of a solid density sample. This is achieved using heating drivers such as hot electrons from direct intense pulsed laser irradiation of a sample [6-8], ultra-bright x-rays from next generation light sources [9,10], and MeV pulsed ions. Ion pulses sufficient for heating to WDM temperatures can be achieved at accelerator facilities [11], or by pulsed laser acceleration [12,13], with the later delivering ions in a much shorter pulse (picoseconds vs nanoseconds), rapidly heating targets of several micron thickness volumetrically to several eV temperatures over an area of > 100 μm.

In this letter, we present measurements of the temperature and expansion rate of copper flash heated using protons generated from ultra-intense laser solid interactions. We heated solid density copper to temperatures ranging from 5 to 10 eV on a picosecond timescale and measured the resulting dynamic copper plasma similar to recent experiments on warm dense aluminum [8,14-16]. Copper and other transition metals are interesting candidates for EOS study, in part because of the complexities arising from their orbital structure [17].

The experiment was performed at the University of Texas at Austin on the GHOST laser, a 17 TW glass and OPCPA laser delivering 2 J of energy in a 115 fs (FWHM) pulse, with a shot rate of up to 1 per minute. To generate the proton beams we used an f/3 off-axis parabolic mirror to focus the laser pulse to a 6 μm diameter spot, yielding a peak intensity of $4x10^{19}$ W/cm^2. This intense focal spot interacted with a 1 μm thick copper *source* foil to produce up to 6×10^{12} protons with a cutoff energy of ~6 MeV and an average energy of ~2 MeV, through the Target Normal Sheath Acceleration (TNSA) mechanism [18,19]. The energy conversion efficiency from laser energy to protons above 300 keV was around 3% yielding 60 mJ in the proton pulse, enough to heat a 1 μm thick copper *sample* foil placed 200 μm from the target to temperatures approaching 10 eV. The source and sample were produced by microfabrication techniques to achieve mirror-like flatness (< 300 nm deviation) with very precise spacing (± 5 μm) and thickness (± 100 nm). FIG. 1 illustrates the experimental layout.

The proton spectra were measured using a calibrated, compact Thomson spectrometer in which signals were registered on imaging plates [20]. This allowed the various accelerated ion species to be distinguished, showing that most of the ions measured were H^+ (protons). The transmitted ion energy spectra were measured on each data shot. To extrapolate spectra below the cutoff energy on shots with a sample foil, several shots were taken without a sample foil. Also with the sample foil removed, we measured a half angle of approximately 10° in the proton divergence using radiochromic film (RCF), a measurement that required the integration of multiple shots because of low proton count in the sensitivity range of the RCF.

We used an absolutely calibrated Streaked Optical Pyrometry (SOP) [11,12,15,21] system to measure the time-resolved spectral radiance at the back surface of the heated sample. The system employed a Hamamatsu C7700 high dynamic range ultrafast streak camera imaging 400 nm light from the heated target. Details of the system calibration are given in Ref. [22]. The rear surface of the heated sample was imaged with an f/4.37 achromatic lens giving approximately 1:1 magnification to the streak camera slit. A 400 nm; 10 nm bandwidth interference filter was placed directly in front of the slit. This diagnostic measured the light emitted by the heated Cu slab with 1-D spatial resolution of 14 μm and temporal resolution of 5 picoseconds. From the image intensity of the light, the cone angle, and the spectral transmission of the collection optics, we measured the radiance at the target as a function of time.

We measured the expansion at the back surface of the proton heated Cu sample using Fourier Domain Interferometry (FDI) [15,23-25]. A fraction of the laser energy was picked off at an early stage of amplification and compressed independently to the main pulse, leaving a linear chirp of 2.4 ps/nm, which correlated time to wavelength in a ~50 ps window. The probe was reflected with S polarization from the back surface of the heated sample, which was imaged to a Michelson interferometer referencing the heated region with a spatially separated unheated region and relay imaged to the slit of a spectrometer, with fringes falling perpendicular to the slit. In this way, we measured the phase shift to within a fraction of the probe wavelength with temporal resolution of < 1 ps, and 1-dimensional spatial resolution better than 10 μm. Reference FDI images of the unheated sample were taken prior to every shot to establish the background phase.

The measurements made by the SOP and FDI are indicative of the temperatures and pressures of the heated material, respectively, while the measurement of the Thomson spectrometer determines the rate of deposition of internal energy into the sample as it is heated to a WDM plasma. To connect these measurements to the equation of state, we employed the 1-D radiative Lagrangian hydrodynamics code HYADES [26] to simulate the heating and expansion of the solid density sample foil. HYADES provides built-in EOS models but also accepts external EOS data tables for electron and ion internal energy and pressure as well as opacity, average ionization state, and other quantities. The use of a 1-D code is justified here because the measured expansion, up to ~1 – 2 μm, is far smaller than the transverse scale: the spatial heating profile is Gaussian-like with width greater than 100 μm.

We derived the energy inputs to the simulations from the measured proton spectra, which was adjusted and extrapolated to cut-off energies for shots with a sample foil in place. We used data tables for stopping power in cold Cu [27] to determine the energy deposition as a function of depth in the material and proton energy, and the transit time of each proton energy over the 200 μm vacuum gap to convert this to a function of time and depth. The Thomson spectrometer measures protons per MeV per steradian at the entrance to the spectrometer, but because TNSA protons originate from an extended source of 10s of microns [19], we estimated the intensity at the sample using a "virtual point source" origin for the ions, positioned approximately 100 μm behind the actual source target. The spatial scale of heating observed by the SOP and FDI were consistent with these assumptions, and the RCF measured cone angle. However, different angular spreads are expected at different energies [28], which could not be distinguished with the RCF measurement for the important energies below 2 MeV. The use of cold stopping powers is another approximation. However, for the temperatures observed in this experiment, the deviation from cold stopping powers should be small [29,30]. Overall, we estimated an uncertainty in the scaling of the energy deposition intensity of ±35%.

The HYADES simulations were run for at least 110 ps after the arrival of the laser pulse, approximately the expansion timescale for the full foil thickness. From each simulation of a proton heated foil we could calculate the expected response of the SOP and FDI.

We calculated the SOP signal using techniques appropriate for a short, dense, highly refractive plasma gradient [31,32]. Using a Helmholtz solver at both P and S polarizations to calculate the absorption profile, we calculate the emission considering the thermal gradient as outlined in Ref. [32]. Most of the thermal emission occurs near the

critical layer of electron density ~ 6.0×10^{21} cm^{-3}, and the thermal gradient at the lower densities is slow. The dielectric function used in the Helmholtz solver was derived from a Drude calculation.

In the figures we express the signal of the SOP in terms of a brightness temperature (BT) in eV, via Planck's formula [33]. Although simulations show that the peak BT is close to the peak temperature at the critical density surface for 400 nm (e.g. emissivity is near 1), we note that the peak BT is shown in the simulations to be a factor of 1.5 to 2.5 less than the peak temperature in the center of the sample [22], meaning that the measured brightness temperatures of > 5 eV presented here correspond to central temperatures of ~10 eV. Simulations of brightness temperature vs time for the same ion input and various EOS models are presented in FIG. 2.

We performed simulations using five different equation of state models for copper. First was an ideal gas model, with pressure simply represented as $P = (Z^*+1)n_ikT$, where Z* is the ionization level as determined by a Thomas Fermi model and n_i is the ion density. Next was SESAME table 3333 [34], an early global EOS model constructed from a patchwork of six theoretical models, with interpolations at their borders and over regions where none of them model were applicable. In this construction, the region of moderate density (.01 to 10 x ρ_{solid}) and temperature (1 – 100 eV) is mostly covered by interpolation. Third we used the "quotidian" QEOS model [35], which is a global, thermodynamically consistent EOS by design, dividing Helmholtz free energy into three parts: a cold curve, ion thermal, and electron thermal contributions, and using it to calculate the thermodynamic quantities. The electron thermal part is calculated using a Thomas Fermi model while the ion part from the Cowan EOS [35], which spans from a Debeye-Grunesian EOS in the solid phase to ideal gas at high temperature. The cold curve is designed to match the measured bulk modulus of the solid material, which is taken as an input. The more modern equations of state considered here all follow the same additive construction of the EOS from three free energy functions, with various levels of sophistication in the constituent models. SESAME tables 3337 [36] are constructed using a Thomas-Fermi-Dirac electron thermal EOS, the Johnson ionic model [37], which is similar to the Cowen models with improvements to melting and liquid states, and a cold curve based on stabilized Jellium near solid density. RESEOS [38] uses an electron thermal model adapted from Inferno (a precursor to Purgatorio), an ideal gas ionic model, and a semi-empirical cold curve. The XEOS [39] tables for copper use the average-atom Purgatorio model for electrons, a similar ionic model to SESAME 3337 and QEOS, and a cold curve constructed similarly to QEOS's. Though XEOS and RESEOS follow similar average atom model constructions for the electron EOS, the use of a simple ideal gas ionic model in RESEOS leads to a substantially lower pressure gradients near solid density and few eV temperatures, reflected in the simulations below.

A consistent and accurate calculation of the Drude dielectric function for a given EOS requires knowledge of the associated average ionization state Z*. Unfortunately, this is not always included with EOS tables. For our simulations, only QEOS had a unique self-consistent determination of Z*, while we were forced to use a separate Thomas Fermi calculation, built into HYADES, for the SESAME EOS and ideal gas runs. For average atom based models XEOS and RESEOS, the description of electronic structure is more complex and so Z* can be defined in several ways, based on the solutions of the wave equations. The three used here are defined in Ref. [17]: For XEOS, we obtained tables for Z_{bg} and Z_{fc}, where Z_{bg} ("background") represents strictly those electrons in the continuum portion of the wave function, and Z_{fc} ("free charge") includes also quasi-bound and resonant states that are technically unbound (pressure ionized). Z_{bg} is likely to be more appropriate for the Drude calculation. For RESEOS we used Z_{ws}, the density of electrons at the surface of the ion sphere multiplied by its volume, which is very close to Z_{bg} for our conditions. In the figures below, simulations for XEOS using both Z_{bg} and Z_{fc} are presented, to illustrate the significance of this choice.

The FDI measures the change in position of the critical density surface for the probe wavelength and incident angle as a function of time. In this case, the reflection surface occurs at an electron density of 9.8×10^{20} cm^{-3}. Outward motion of a reflecting surface by Δx imparts a phase shift of $\Delta\varphi = -2\, k_0\, \Delta x \cos\theta$ in a probe with wavelength λ_0 incident at an angle of θ, where $k_0=2\pi/\lambda_0$. However, the probe must pass through under-dense plasma in front of the critical layer, which also affects the phase. To account for this effect we again employed a Helmholtz wave solver,

this time to simulate the phase shift incurred by the probe laser in reflection as a function of time [40]. Here we present the measured and calculated values in terms of the "apparent expansion" and "apparent velocity" of a bare reflecting surface that would give the same phase shift. For our conditions the apparent velocity is calculated to be from 5-15% greater than the velocity of the critical density surface, and up to 5% different from a basic ray tracing approximation [40].

Simulations give the expected expansion, as measured by the FDI, for a given BT measurement of the SOP, for various EOS models. By scaling the measured proton spectra within the estimated uncertainty of energy deposition, we could produce a simulation for each EOS model that fit the measured SOP trace well, as shown for an example shot in FIG. 3(A). Note that the discrepancy from the measured SOP signal at early times, before the peak, consists mostly of optical transition radiation from electrons and the fastest protons passing through the sample [41]. This OTR burst is short and can be distinguished spatially because of the angle between laser forward and target normal directions. We note also the poor fit of the ideal gas calculation after the peak. For the same simulations and the same data shot, FIG. 3(B) shows the expansion measured at the center of the heated region along with the calculated apparent expansions. We observe in measurement and simulations that the expansion reaches a roughly constant velocity at around 30-40 ps. In this example the final slope of the measured expansion is, within uncertainty, consistent with the simulated curves of XEOS, for both ionization models, and Sesame 3337.

The relationship between the peak brightness temperature (BT) and linear velocity is plotted for measurements and simulations in FIG. 4. Each measurement point represents a single shot. Error bars in the velocity direction result from a loss of fringe contrast as reflectivity decreases sharply from the heated target. Error in the BT axis is the estimated systematic and random error in the radiance measurement. We note that it was unnecessary to vary the laser pulse parameters to cover this temperature range: the natural shot-to-shot variation in the proton beam was enough. Each curve in the figure was generated from a large set of simulations using a given EOS model, and the energy inputs were derived from the set of measured ion spectra taken over the course of the campaign. Multiple scalings of each proton spectrum were used, covering the range of the uncertainty in the absolute energy deposition. For a given EOS model, the segments of the curve generated by the different spectra overlap almost exactly, despite wide differences in average ion energy and cutoff energy, and so each EOS can be presented as a single curve. This also held true for moderate changes to the vacuum gap distance (± 10 μm).

The position in FIG. 4 of each curve depends primarily on the pressures and the ionization levels given by the associated EOS. Higher pressure drives faster expansion velocities and push the curve upward, while ionization level determines the location of the critical density surface relative to the ion density profile, with higher ionization levels leading to the probing of lower ion density layers, which are moving at higher velocity. Differences between the pressures predicted by the various EOS models were small near the critical surfaces, but large in the central higher density layers, with QEOS and Sesame 3337 predicting the highest pressures, and Sesame 3333 and RESEOS having the lowest. The tabulated ionization levels for XEOS and REOS are somewhat lower than those calculated by the Thomas Fermi model, explaining the position of their curves toward the lower right of FIG. 4. The difference between XEOS with Z_{fc} or Z_{bg} being used in the Drude calculation isolates the influence of the ionization level calculation.

We find that none of the advanced EOS models fit the measurements very well across the full range of temperatures we explored. A larger data set, ideally with improved measurement accuracy in the expansion measurement, will be needed to provide better statistics to significantly constrain the EOS models. Also, this technique requires that the prediction of the dielectric function in the expanding plasma be well estimated. For the Drude model, this requires an appropriate self-consistent determination of the density of free electrons, but one might also consider more advanced calculations of the dielectric functions [42], as they are critical to optical measurements.

In conclusion, we have presented an experiment in which we probed a largely unexplored region of temperature-density space of warm dense copper by measuring the expansion and temperature of a proton-heated solid. We

present a useful means to reduce a large set of shots to a single plot for straightforward benchmarking of various EOS models. Large differences between the models for this temperature range show an opportunity for improvement as more data are collected.

We gratefully acknowledge David Young and Philip Sterne of LLNL in helping us obtain and understand the XEOS tables for copper and for generating associated ionization tables, Scott Crockett of LANL for providing SESAME tables and information about their construction, Anton Ovechkin for providing RESEOS tables for copper, and Jon Larsen of Cascade Applied Sciences, Inc., for support of HYADES. This work was supported by the U.S. Department of Energy National Nuclear Security Administration under Cooperative agreement DE-NA0002008.

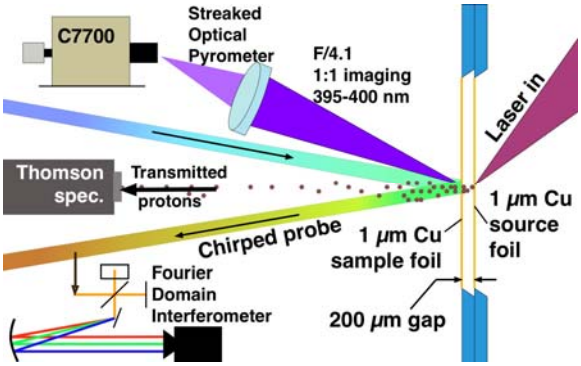

FIG. 1. Schematic of experimental layout. Laser is incident at 45°; FDI probe angle is 9.46°; SOP viewing angle is 22.5°; Thomson measures ions in source target normal direction.

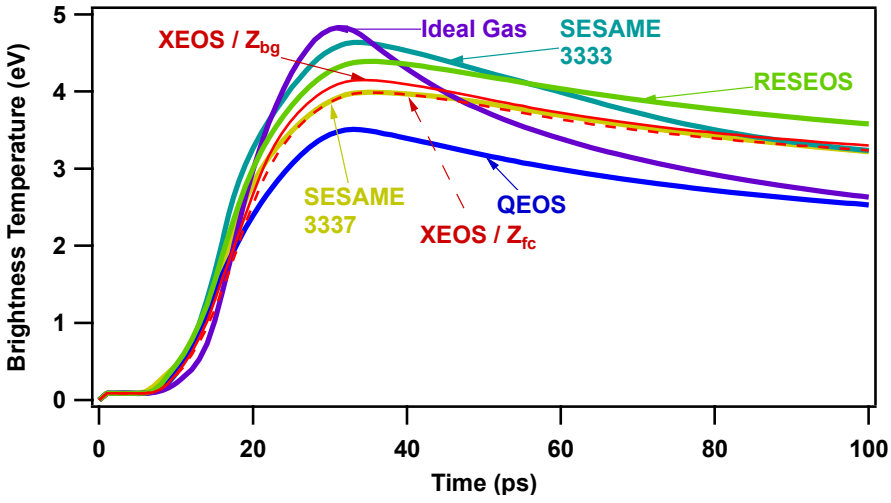

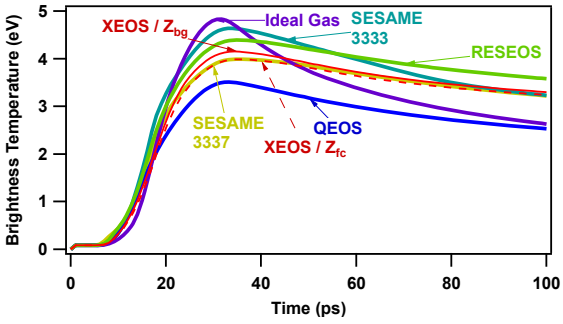

FIG. 2. Brightness temperature versus time for the six models with the same heating profile, as derived from the measured ions of a specific shot. XEOS results are shown for two different definitions of Z* being used to calculate the dielectric function for the Helmholtz equation.

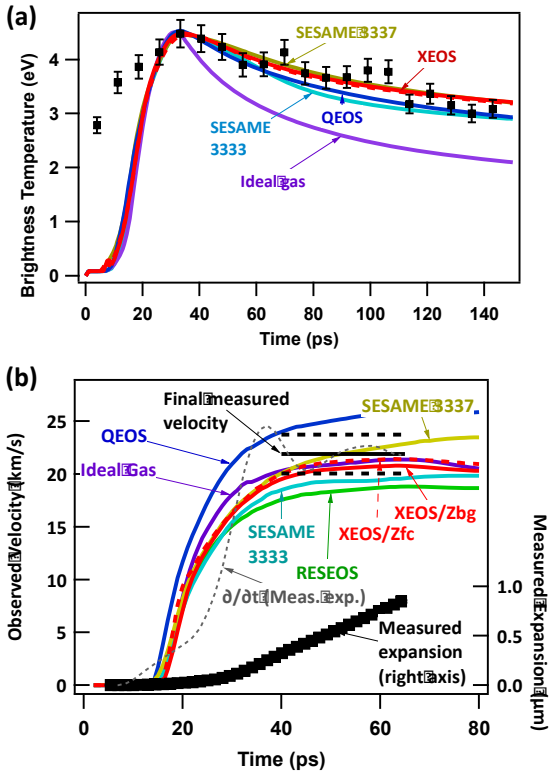

FIG. 3. Measured and simulated brightness temperature (A) and expansion rate (B). Measurements (black curves and points) are taken in the central region of heating. One simulation is given for each of six models, where the energy inputs are individually scaled such that the peak BT matches that of the measurement. Measured expansion and the derivative of the smoothed curve are shown, along with the determination of final velocity.

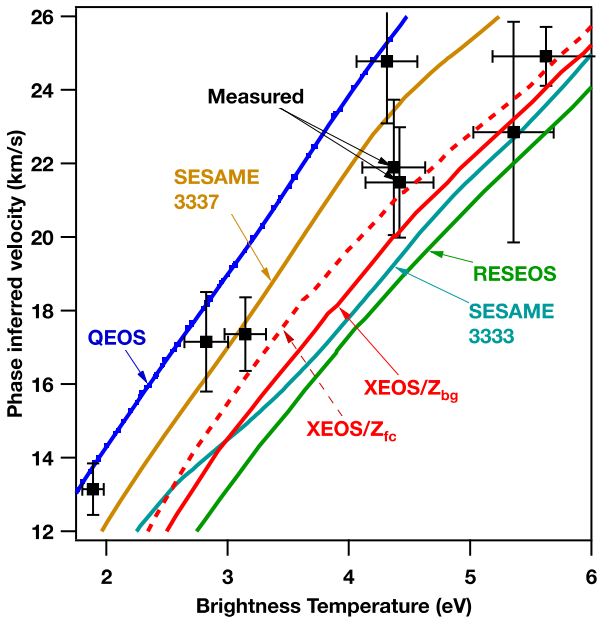

FIG. 4: Final expansion velocity vs brightness temperature for measurements and simulations. Curves show simulations using various equation of state models. Each measured data point represents a single shot, with error bars based on the estimated certainty of each measurement. For QEOS, individual simulations are shown as dots to show the maximum deviations from the curve.

[1] F. Graziani, M. P. Desjarlais, R. Redmer, and S. B. Trickey, editors, *Frontiers and Challenges in Warm Dense Matter* (Springer International Publishing, Cham, 2014).

[2] V. E. Fortov and I. V. Lomonosov, Shock Waves **20**, 53 (2009).

[3] A. Benuzzi, T. Lower, M. Koenig, B. Faral, D. Batani, D. Beretta, C. Danson, and D. Pepler, Phys. Rev. E **54**, 2162 (1996).

[4] R. Cauble, L. B. Da Silva, P. M. Celliers, G. W. Collins, and D. M. Gold, in *High-Field Science* (Springer US, Boston, MA, 2000), pp. 41–50.

[5] D. Batani, A. Morelli, M. Tomasini, A. Benuzzi-Mounaix, F. Philippe, M. Koenig, B. Marchet, I. Masclet, M. Rabec, C. Reverdin, R. Cauble, P. Celliers, G. Collins, L. da Silva, T. Hall, M. Moret, B. Sacchi, P. Baclet, and B. Cathala, Phys. Rev. Lett. **88**, 235502 (2002).

[6] B. I. Cho, K. Engelhorn, A. A. Correa, T. Ogitsu, C. P. Weber, H. J. Lee, J. Feng, P. A. Ni, Y. Ping, A. J. Nelson, D. Prendergast, R. W. Lee, R. W. Falcone, and P. A. Heimann, Phys. Rev. Lett. **106**, 167601 (2011).

[7] A. J. Nelson, J. Dunn, J. Hunter, and K. Widmann, Appl. Phys. Lett. **87**, 154102 (2005).

[8] P. Antici, L. Gremillet, T. Grismayer, P. Mora, P. Audebert, M. Borghesi, C. A. Cecchetti, A. Mancic, and J. Fuchs, Phys. Plasmas **20**, 123116 (2013).

[9] S. M. Vinko, O. Ciricosta, B. I. Cho, K. Engelhorn, H. K. Chung, C. R. D. Brown, T. Burian, J. Chalupský, R. W. Falcone, C. Graves, V. Hájková, A. Higginbotham, L. Juha, J. Krzywinski, H. J. Lee, M. Messerschmidt, C. D. Murphy, Y. Ping, A. Scherz, W. Schlotter, S. Toleikis, J. J. Turner, L. Vyšín, T. Wang, B. Wu, U. Zastrau, D. Zhu, R. W. Lee, P. A. Heimann, B. Nagler, and J. S. Wark, Nature (London) **482**, 59 (2012).

[10] A. Lévy, P. Audebert, R. Shepherd, J. Dunn, M. Cammarata, O. Ciricosta, F. Deneuville, F. Dorchies, M. Fajardo, C. Fourment, D. Fritz, J. Fuchs, J. Gaudin, M. Gauthier, A. Graf, H. J. Lee, H. Lemke, B. Nagler, J. Park, O. Peyrusse, A. B. Steel, S. M. Vinko, J. S. Wark, G. O. Williams, D. Zhu, and R. W. Lee, Phys. Plasmas **22**, 030703 (2015).

[11] F. M. Bieniosek, J. J. Barnard, A. Friedman, E. Henestroza, J. Y. Jung, M. A. Leitner, S. Lidia,

B. G. Logan, R. M. More, P. A. Ni, P. K. Roy, P. A. Seidl, and W. L. Waldron, J. Phys. Conf. Ser. **244**, 032028 (2010).
[12] P. K. Patel, A. J. Mackinnon, M. H. Key, T. E. Cowan, M. E. Foord, M. Allen, D. F. Price, H. Ruhl, P. T. Springer, and R. Stephens, Phys. Rev. Lett. **91**, 125004 (2003).
[13] W. Bang, B. J. Albright, P. A. Bradley, E. L. Vold, J. C. Boettger, and J. C. Fernández, Phys. Rev. E **92**, 063101 (2015).
[14] P. Antici, J. Fuchs, S. Atzeni, and A. Benuzzi, J. Phys. IV France **133**, 1077 (2006).
[15] G. M. Dyer, A. C. Bernstein, B. I. Cho, J. Osterholz, W. Grigsby, R. Shepherd, Y. Ping, K. Widmann, and T. Ditmire, Phys. Rev. Lett. **101**, 15002 (2008).
[16] A. Mancic, J. Robiche, P. Antici, P. Audebert, C. Blancard, P. Combis, F. Dorchies, G. Faussurier, S. Fourmaux, M. Harmand, R. Kodama, L. Lancia, S. Mazevet, M. Nakatsutsumi, O. Peyrusse, V. Recoules, P. Renaudin, R. Shepherd, and J. Fuchs, High Energy Density Phys. **6**, 21 (2010).
[17] P. A. Sterne, S. B. Hansen, B. G. Wilson, and W. A. Isaacs, High Energy Density Phys. **3**, 278 (2007).
[18] S. C. Wilks, A. B. Langdon, T. E. Cowan, M. Roth, M. Singh, S. Hatchett, M. H. Key, D. Pennington, A. MacKinnon, and R. A. Snavely, Phys. Plasmas **8**, 542 (2001).
[19] T. E. Cowan, J. Fuchs, H. Ruhl, Y. Sentoku, A. Kemp, P. Audebert, M. Roth, R. Stephens, I. Barton, A. Blazevic, E. Brambrink, J. Cobble, J. C. Fernández, J. C. Gauthier, M. Geissel, M. Hegelich, J. Kaae, S. Karsch, G. P. Le Sage, S. Letzring, M. Manclossi, S. Meyroneinc, A. Newkirk, H. Pépin, and N. Renard-LeGalloudec, Nucl. Instrum. Methods Phys. Res. A **544**, 277 (2005).
[20] J. T. Morrison, C. Willis, R. R. Freeman, and L. Van Woerkom, Rev. Sci. Instr. **82**, 033506 (2011).
[21] P. Antici, J. Fuchs, S. Atzeni, A. Benuzzi, E. Brambrink, M. Koenig, J. Schreiber, A. Schiavi, and P. Audebert, J. Phys. IV France **133**, 1077 (2006).
[22] S. H. Feldman, Isochoric Heating of Copper to Warm Dense Matter State Using Protons Produced Through Laser Solid-Laser Interactions, ProQuest Dissertations And Theses; Thesis (Ph.D.)--The University of Texas at Austin, 2013.
[23] S. Rebibo, J. P. Geindre, P. Audebert, G. Grillon, J. P. Chambaret, and J. C. Gauthier, Laser Part. Beams **19**, 67 (2001).
[24] J. P. Geindre, P. Audebert, S. Rebibo, and J. C. Gauthier, Opt. Lett. **26**, 1612 (2001).
[25] P. Antici, L. Gremillet, T. Grismayer, P. Mora, P. Audebert, M. Borghesi, C. A. Cecchetti, A. Mancic, and J. Fuchs, Phys. Plasmas **20**, 123116 (2013).
[26] J. T. Larsen, S. M. Lane, and S. Lane, J. Quant. Spectrosc. Radiat. Transfer (1994).
[27] N. US Department of Commerce, M. Berger, J. Coursey, M. Zucker, and J. Chang, *ESTAR, PSTAR, and ASTAR: Computer Programs for Calculating Stopping-Power and Range Tables for Electrons, Protons, and Helium Ions (Version 1.2.3)*, [Online] Available: http://physics.nist.gov/Star (National Institute of Standards and Technology, Gaithersburg, MD, 2005).
[28] S. Ter-Avetisyan, M. Schnurer, P. V. Nickles, W. Sandner, T. Nakamura, and K. Mima, Phys. Plasmas **16**, 043108 (2009).
[29] M. Gauthier, C. Blancard, S. N. Chen, B. Siberchicot, M. Torrent, G. Faussurier, and J. Fuchs, High Energy Density Phys. **9**, 488 (2013).
[30] J. Kim, B. Qiao, C. Mcguffey, M. S. Wei, P. E. Grabowski, and F. N. Beg, (n.d.).
[31] P. Celliers and A. Ng, Phys. Rev. E **47**, 3547 (1993).
[32] M. Basko, T. Löwer, V. N. Kondrashov, A. Kendl, R. Sigel, and J. Meyer-Ter-Vehn, **56**, 1019 (1997).
[33] J. Mahan, *Radiation Heat Transfer: a Statistical Approach* (Wiley, 2002).
[34] K. S. Trainor, Journal of Applied Physics **54**, 2372 (1983).
[35] D. A. Young and E. M. Corey, **78**, 3748 (1995).

[36] J. H. Peterson, K. G. Honnell, C. Greeff, J. D. Johnson, J. Boettger, and S. Crockett, in *AIP Conf. Proc. 1426* (AIP, 2012), pp. 763–766.
[37] J. D. Johnson, Int. J. High Pres. Res. **6**, 277 (2006).
[38] A. A. Ovechkin, P. A. Loboda, V. G. Novikov, A. S. Grushin, and A. D. Solomyannaya, High Energy Density Phys. **13**, 20 (2014).
[39] B. Wilson, V. Sonnad, P. Sterne, and W. Isaacs, J. Quant. Spectrosc. Radiat. Transfer **99**, 658 (2006).
[40] P. Blanc, P. Audebert, F. Fallies, J. P. Geindre, J. C. Gauthier, A. Dos Santos, A. Mysyrowicz, and A. Antonetti, J Opt Soc Am B **13**, 118 (1996).
[41] B. Gitter, *Optical Transition Radiation* (UCLA Department of Physics Center for Advanced Accelerators Particle Beam Physics Lab, 1992).
[42] A. A. Ovechkin, P. A. Loboda, and A. L. Falkov, High Energy Density Phys. **20**, 38 (2016).